Electronic Supplementary Material (ESI) for CrystEngComm.

Supporting Information

S1. Structure Characterization.

S1.1. Single crystal X-Ray diffraction (SCXRD).

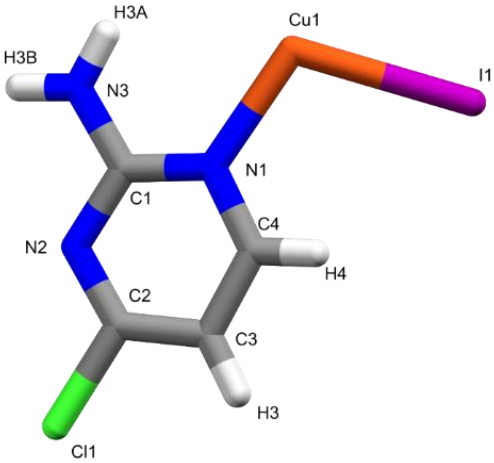

Figure S1. Asymmetric unit of **1D-[Cu(aClpym)I]$_n$** with atoms labelled.

Table S1. Single-crystal data and structure refinement details for compounds **1D-[Cu(aClpym)I]$_n$ (CP1)** at room (RT) and low temperature (LT).

1D-[Cu(aClpym)I]$_n$	**RT**	**LT**
CCDC Number	2111057	2111067
Empirical formula	$C_4H_4ClCuIN_3$	$C_4H_4ClCuIN_3$
Formula weight	319.99	319.99
T (K)	296(2)	100(2)
λ (Å)	0.71073	0.71073
Crystal system	monoclinic	monoclinic
Space group	$P2_1/n$	$P2_1/n$
a (Å)	4.1299(2)	4.1143(15)
b (Å)	16.7869(6)	16.538(5)
c (Å)	11.0839(4)	11.100(3)
α (°)	90	90
β (°)	94.769(3)	94.13(2)
ɣ (°)	90	90
V (Å^3)	765.77(5)	753.3(4)
Z	4	4
ρ_{calc} (g·cm^{-3})	2.776	2.821
μ (mm^{-1})	7.154	7.272
Reflexion collected	1387	1384
Unique data /parameters	1386/92	1384/91
Goodness of fit (*S*)	0.883	1.084
*R*1/*wR*2 [$I > 2\sigma(I)$]	0.0361/0.0888	0.0410/0.1095
*R*1/*wR*2 [all data]	0.0571/0.0961	0.0603/0.1161

Table S2. Bond distances (Å) and bond angles (º) of compound **CP1** at room temperature (RT) and low temperature (LT).

1D-[Cu(aClpym)I]$_n$	**RT**	**LT**
Cu-I1$_{rail}$	2.632	2.634
Cu-I1$^{i}_{rail}$	2.695	2.674
Δ[Cu-I1$_{rail}$]	0.063	0.040
Cu-I1$^{ii}_{rung}$	2.666	2.627
Cu-N1	2.042	2.038
Cu-Cu1^{ii}	2.696	2.688
Cu-Cu1^{iii}	3.360	3.332
Δ[Cu-Cu]	0.664	0.644
I1-Cu1-I1^{i}	101.65	101.63
I1^{i}-Cu1-I1^{ii}	102.37	102.12
I1-Cu1-I1^{ii}	118.84	118.53
Cu1-I1^{i}-Cu1^{iii}	77.63	77.88
Cu1-I1-Cu1^{ii}	61.16	61.47
Cu1^{ii}-I1^{ii}-Cu1^{iii}	101.65	101.63
Dihedral angle [a]	110.90	110.57
Tilt angle [b]	98.73	89.96
Twist angle [b]	44.14	41.62
π···π interactions	3.385	3.361
H-bonding	2.196	2.162

Cu and I atoms have superscripts (i, ii, iii) assigned as shown in Figure 1. **[a]** Dihedral angle between adjacent Cu_2I_2 squares **[b]** Tilt and twist angles of the pyrimidinic ring relative to the propagation direction of the chain.

Table S3. Variation (Δ^{RT-LT}) of bond distances (Å) and bond angles (º) in the double chains Cu-I and variation of π···π and H-bonding interactions between room temperature (RT) and low temperature (LT) of compound **CP1**.

Compound	**1D-[Cu(aClpym)I]$_n$**
Δ[Cu-Cu^{ii}]$^{RT-LT}$	0.008
Δ[Cu-Cu^{iii}]$^{RT-LT}$	0.028
Δ[I1-Cu1-I1^{i}]$^{RT-LT}$	0.020
Δ[I1^{i}-Cu1-I1^{ii}]$^{RT-LT}$	0.250
Δ[I1-Cu1-I1^{ii}]$^{RT-LT}$	0.310
Δ[Cu1-I1^{i}-Cu1^{iii}]$^{RT-LT}$	0.250
Δ[Cu1-I1-Cu1^{ii}]$^{RT-LT}$	0.310
Δ[Cu1^{ii}-I1^{ii}-Cu1^{iii}]$^{RT-LT}$	0.020
Δ[Dihedral angle]$^{RT-LT}$	0.33
Δ[Tilt angle]$^{RT-LT}$	8.77
Δ[Twist angle]$^{RT-LT}$	2.52
Δ[π···π]$^{RT-LT}$	0.024
Δ[H-bonding]$^{RT-LT}$	0.034

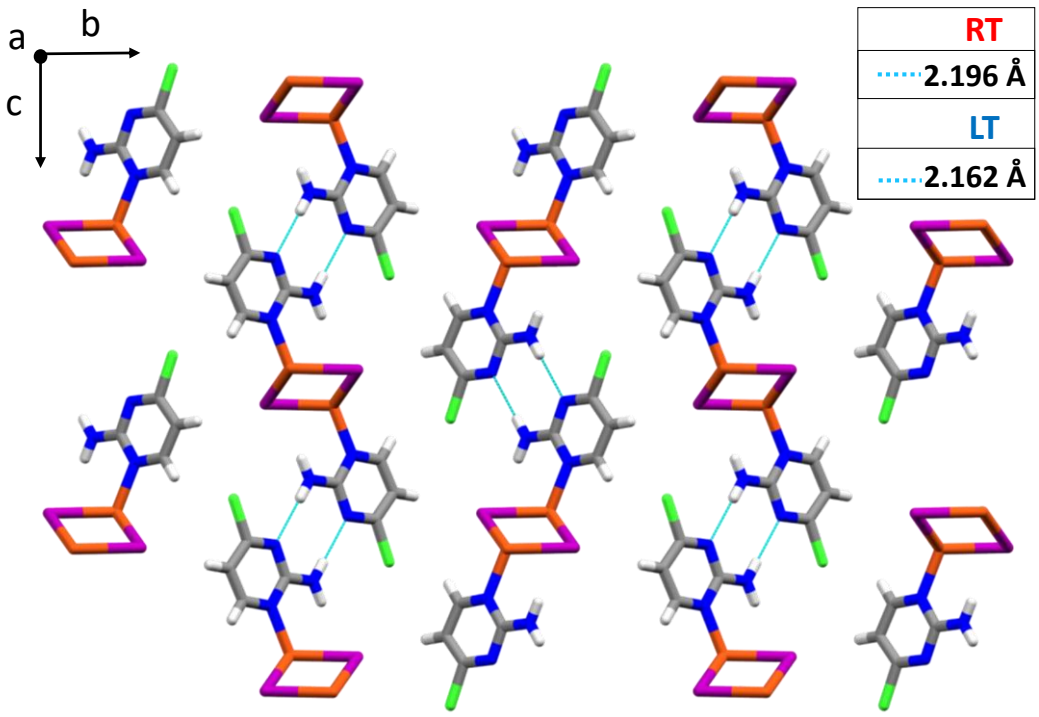

Figure S2. Packing of **1D-[Cu(aClpym)I]$_n$** seen on [100] direction. H: white; I: violet; N: blue; Cu: orange; C: grey and Cl: green. Dashed light blue lines indicate the presence of H-bonding interactions measured at RT (296 K) and LT (100 K).

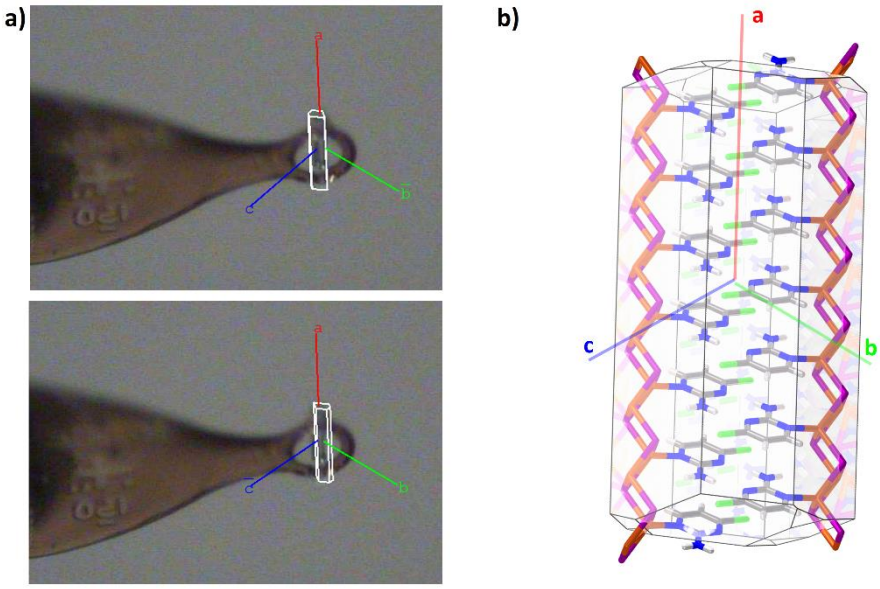

Figure S3. a) Indexing of a two-domain twin crystal rotated 180º of 1D-[Cu(aClpym)I]n with the directions corresponding to the crystallographic axes indicated. **b)** Mercury calculation of BFDH morphology of the structure, which agrees with the real single crystal.

S1.2. X Ray powder diffraction analysis of **1D-[Cu(aClpym)I]n (CP1)**.

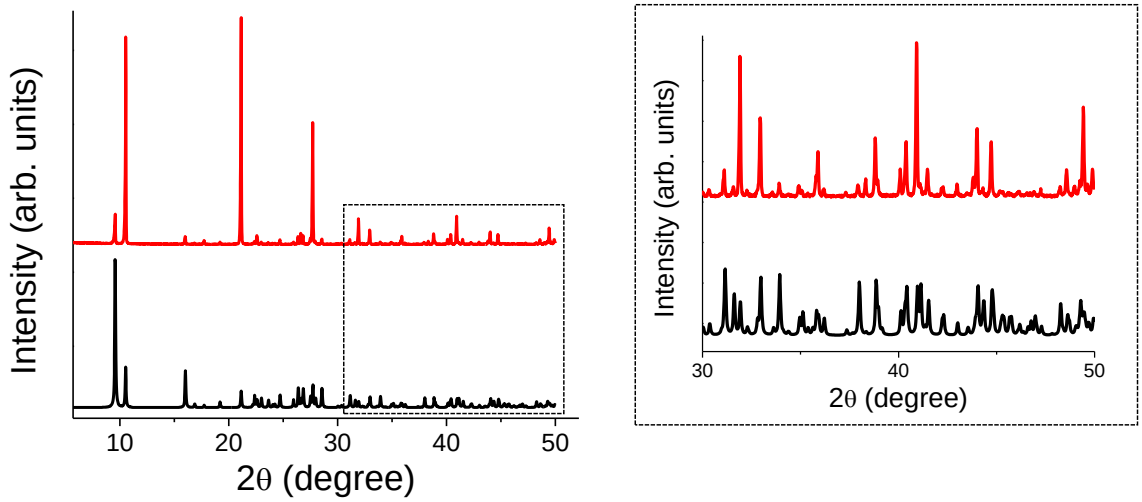

Figure S4. PXRD patterns of **1D-[Cu(aClpym)I]n** (**CP1**) theoretical (black) and experimental (red).

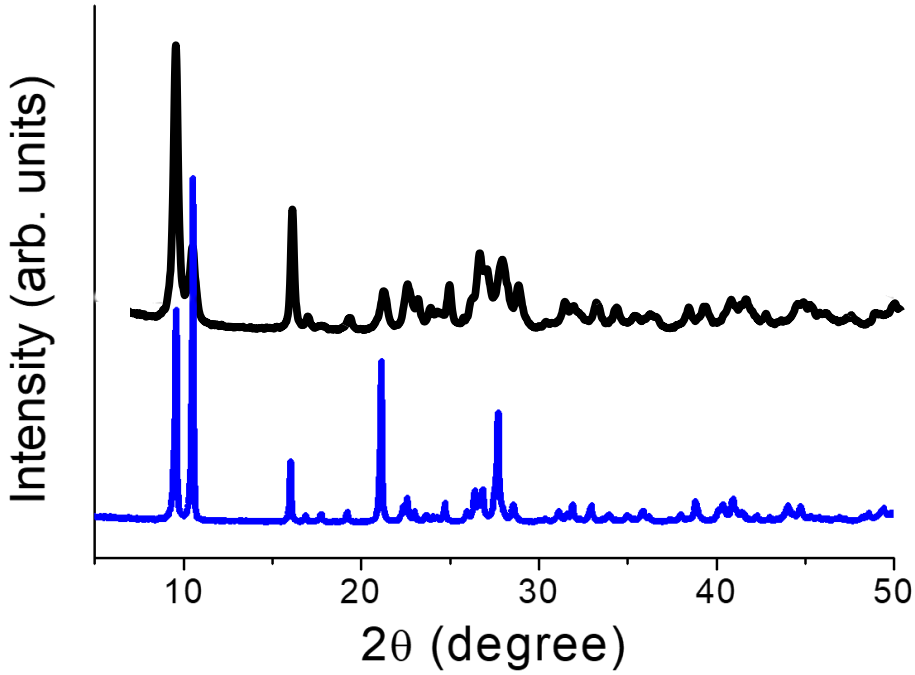

Figure S5. PXRD patterns of **1D-[Cu(aClpym)I]n** at different grinding times**:** 0 minutes (light blue) and 15 minutes (black).

S2. IR Spectra of 1D-[Cu(aClpym)I]n.

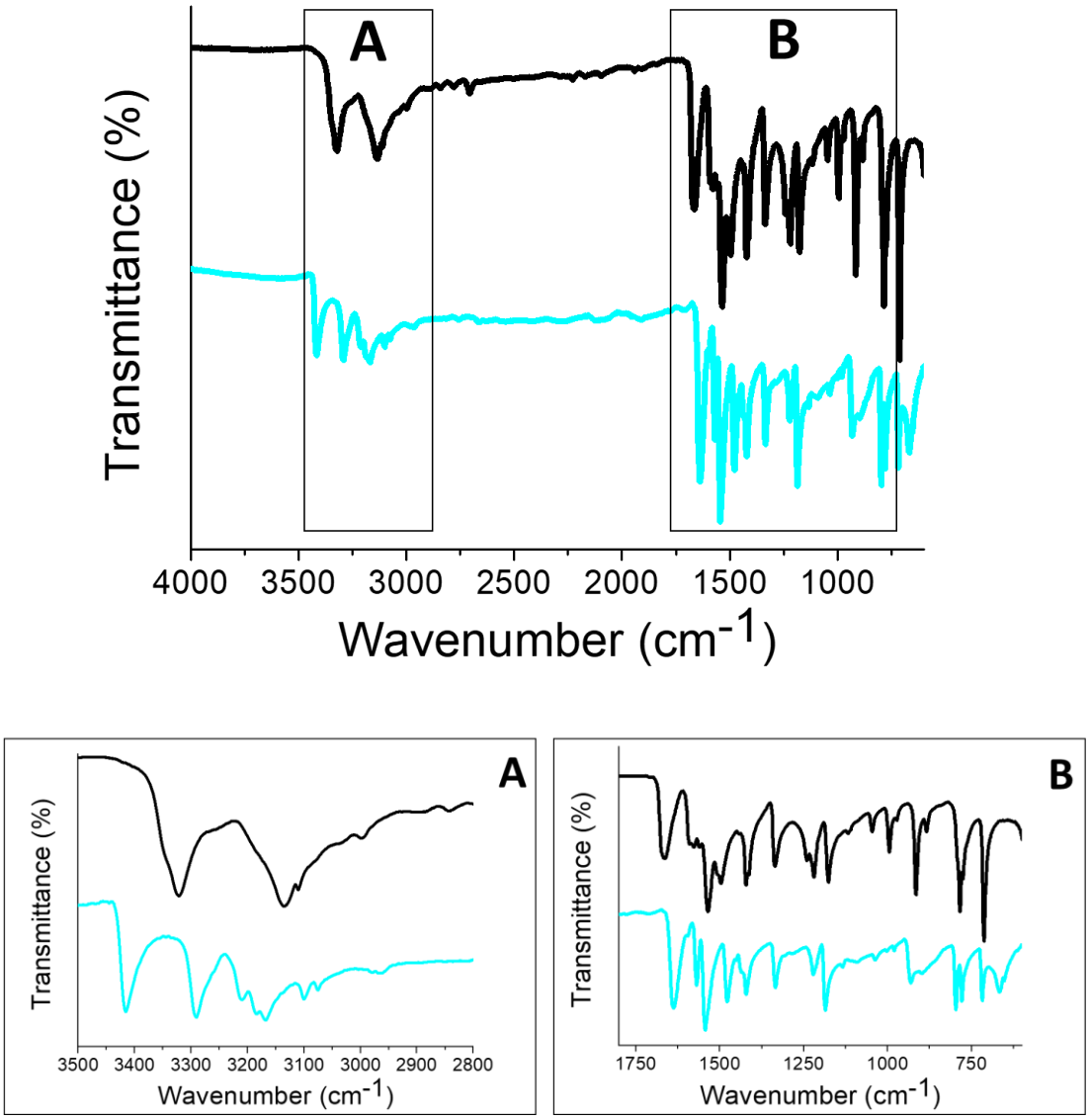

Figure S6. IR Spectrum of 2-amino-4-chloropyrimidine (black) and **1D-[Cu(aClpym)I]$_n$ (CP1)** (light blue): (**A**) 3500-2800 cm^{-1}, (**B**)1800-650 cm^{-1}

S3. Thermogravimetric analysis of 1D-[Cu(aClpym)I]n.

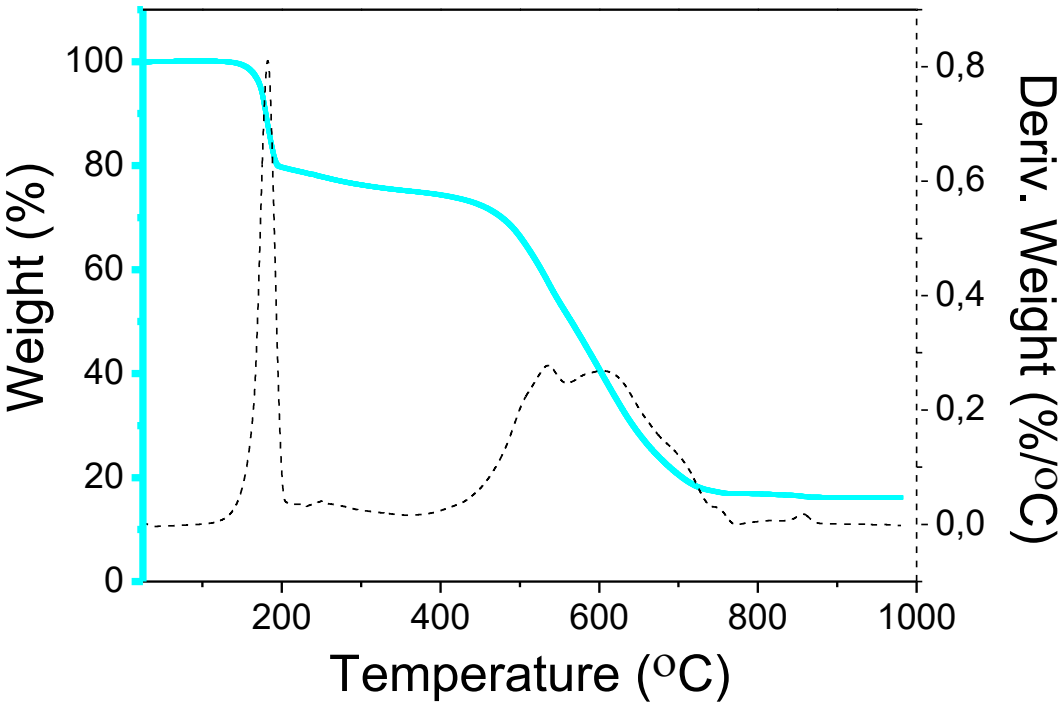

Figure S7. TGA-DTA of **1D-[Cu(aClpym)I]n** (light blue line and black dash**).**

Table S4. Decomposition temperatures, maximum loss weights and residual weights of **1D-[Cu(aClpym)I]n**

Coordination polymer	$T_{5\%}$ (°C)	T_{max} (°C)	D_{max} (%/°C)	W_R (%)
1D-[Cu(aClpym)I]$_n$	174	182	0.8104	16.17

S4. Emission studies of 1D-[Cu(aClpym)I]$_n$.

Table S5. Solid State Luminescence for [CuIL] Coordination Polymers (L= substituted pyrimidine) at room temperature.

Compound	λ_{em} (nm)	Reference
1D[(CuI)(dapym)]$_n$	550	*Inorg Chem* **2021,** *60* (2), 1208.
2D[(Cu_2I_2)(dapym)]$_n$	530	*Inorg Chem* **2021,** *60* (2), 1208
1D[(CuI)(aClpym)]$_n$	468	This work
1D[(Cu_2I_2)(5-mepym)]$_n$	570	J.Am.Chem.Soc., **2015**, 9400
1D[(Cu_2I_2)(5-Brpym)]$_n$	545	J.Am.Chem.Soc., **2014**, 14230

dapym= 2,4-diaminepyrimidine. aClpym = 2,4-aminochloropyrimidine. 5-mepym = 5-methylpyrimidine. 5-Brpym= 5-bromopyrimidine.

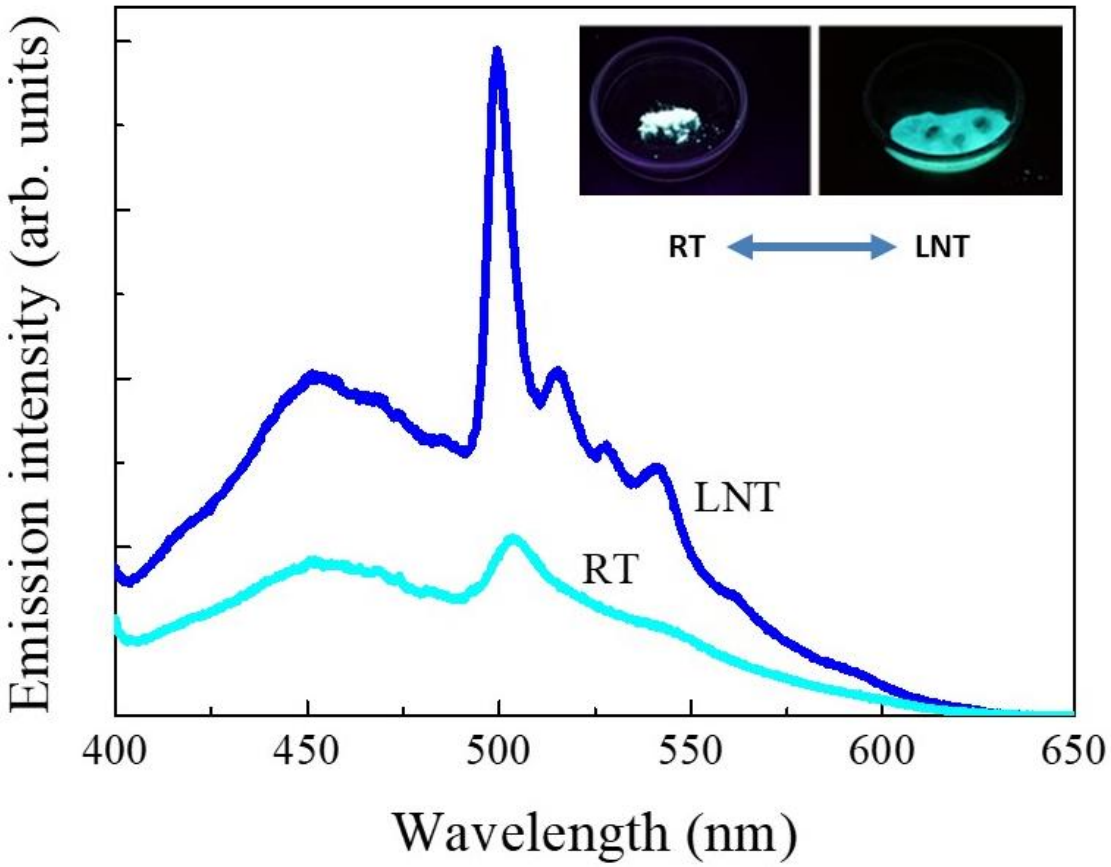

Figure S8. Emission spectrum at λ_{exc}= 356 nm in solid state of ligand 2,4-aminochloropyrimidine (**aClpym)** at: 300 K (light blue line) and 80 K (dark blue line).

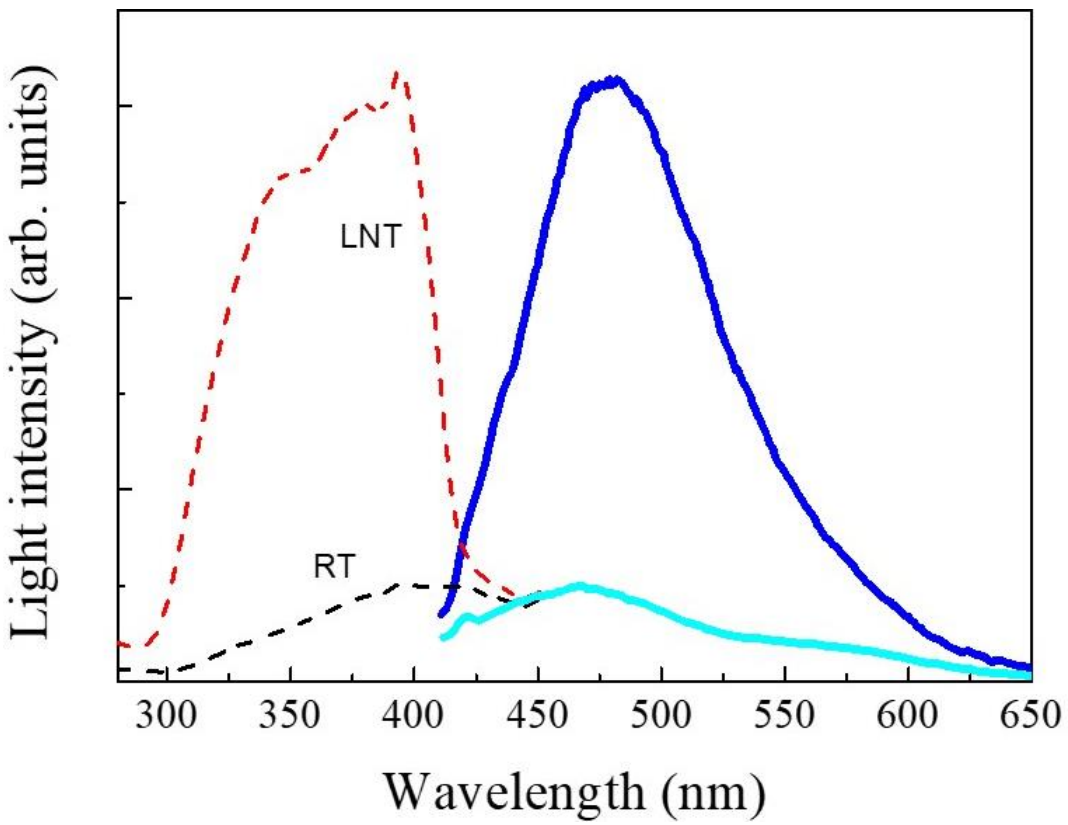

Figure S9. Excitation (λ_{emi} = 480 nm) and emission (λ_{exc} = 390 nm) spectra in solid state of **1D-[Cu(aClpym)I]$_n$** at: 300 K (black dash and light blue line) and 80 K (red dash and dark blue line).

Table S6. Luminescence data for coordination polymer **1D-[Cu(aClpym)I]$_n$** at 300 K and 80 K. Comparatives values of emission wavelength (λ_{emi}), lifetimes (τ_1, τ_2), amplitudes (A_1, A_2), and average lifetime (<τ>), for pulsed excitation at 355 nm.

Compound	T (K)	λ_{exc} (nm)	λ_{emi} (nm)	Emission color	τ_1 (μs)	τ_2 (μs)	$A_1/(A_1+A_2)$	<τ>[a] (μs)
CP1	300	355	470	Blue	0.02	0.08	0.92	0.03
	80	355	480	Light bue	0.03	0.18	0.84	0.11

$$^{a}\langle\tau\rangle = \frac{\int_0^\infty t\,I(t)dt}{\int_0^\infty I(t)dt} = \frac{A_1\tau_1^2 + A_2\tau_2^2}{A_1\tau_1 + A_2\tau_2}$$

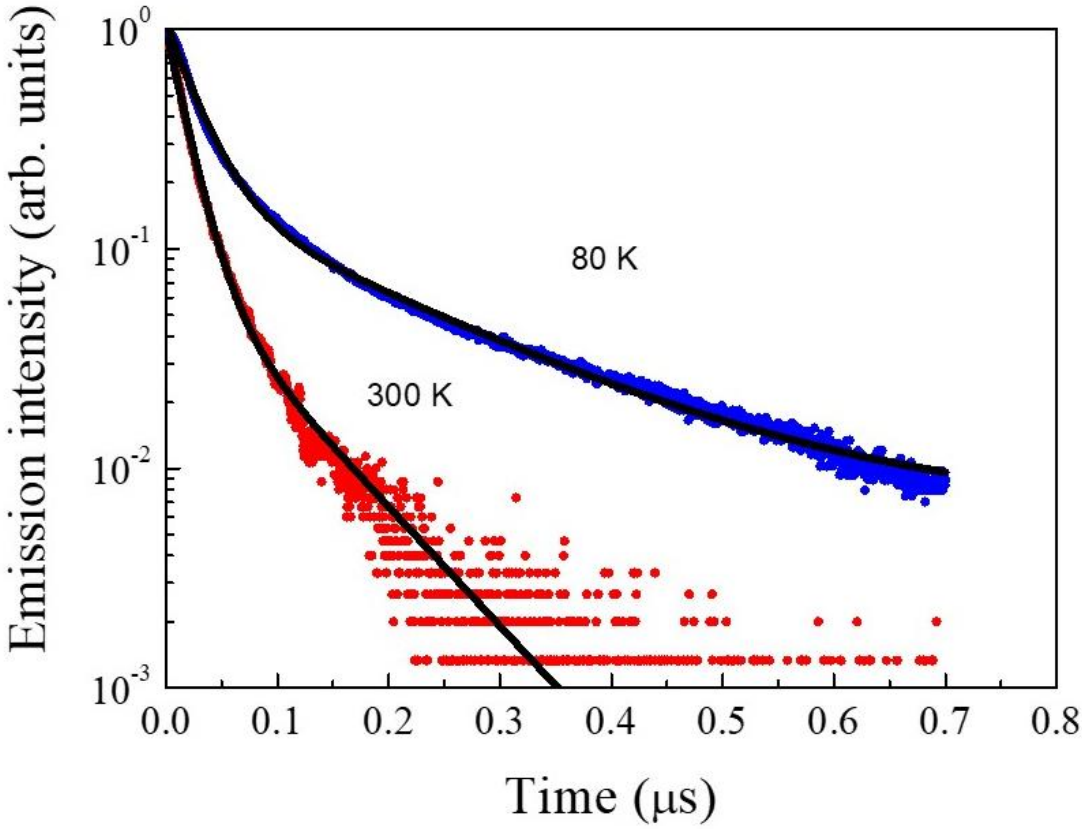

Figure S10. Lifetime of **1D-[Cu(aClpym)I]$_n$** at 80 K (blue circles) and 300 K (red circles). Black lines: fit of the experimental data.

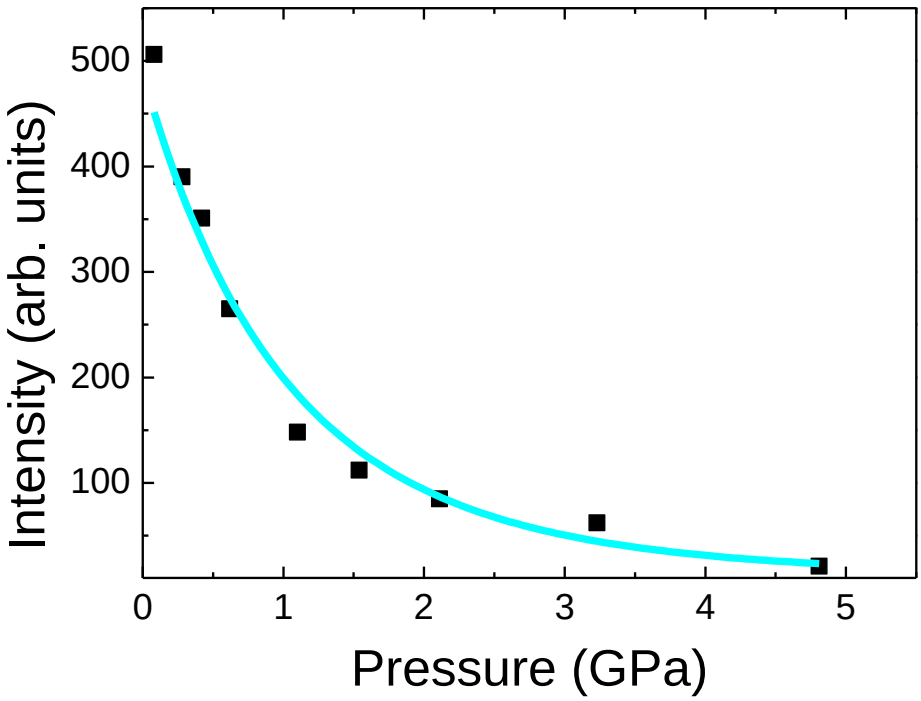

Figure S11. Integrated intensity of **1D-[Cu(aClpym)I]$_n$** obtained at 25 °C under 375 nm laser excitation for different externally applied hydrostatic pressure.

S5. High pressure and EoS analysis of 1D-[Cu(aClpym)I]$_n$ single crystals.

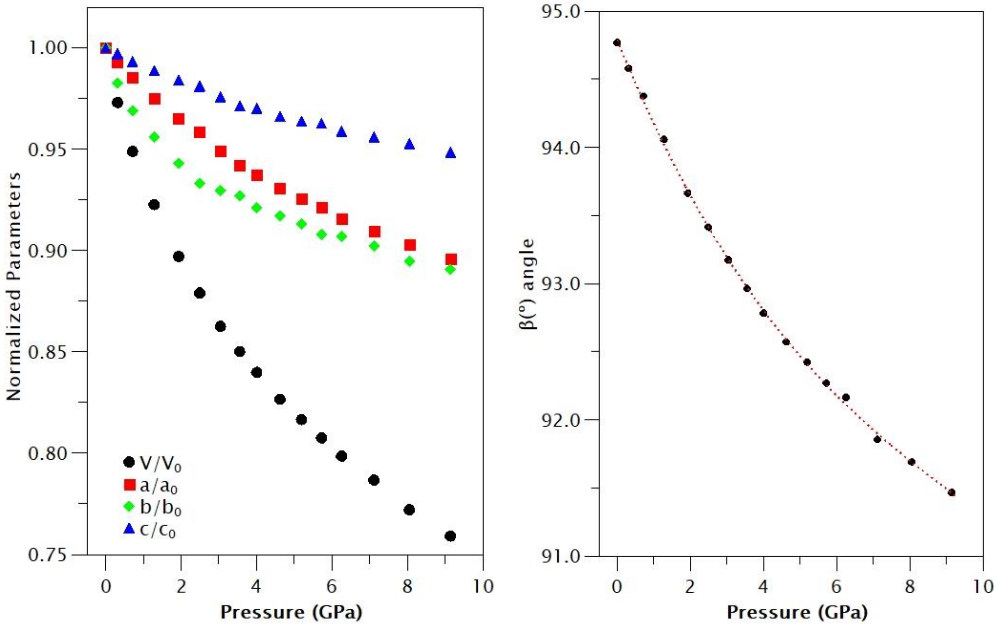

Figure S12. Left: Variation of the cell parameters with pressure. The symbols are bigger than their respective standard deviation. Right: β angle behavior with pressure. The line is only for visualization purpose.

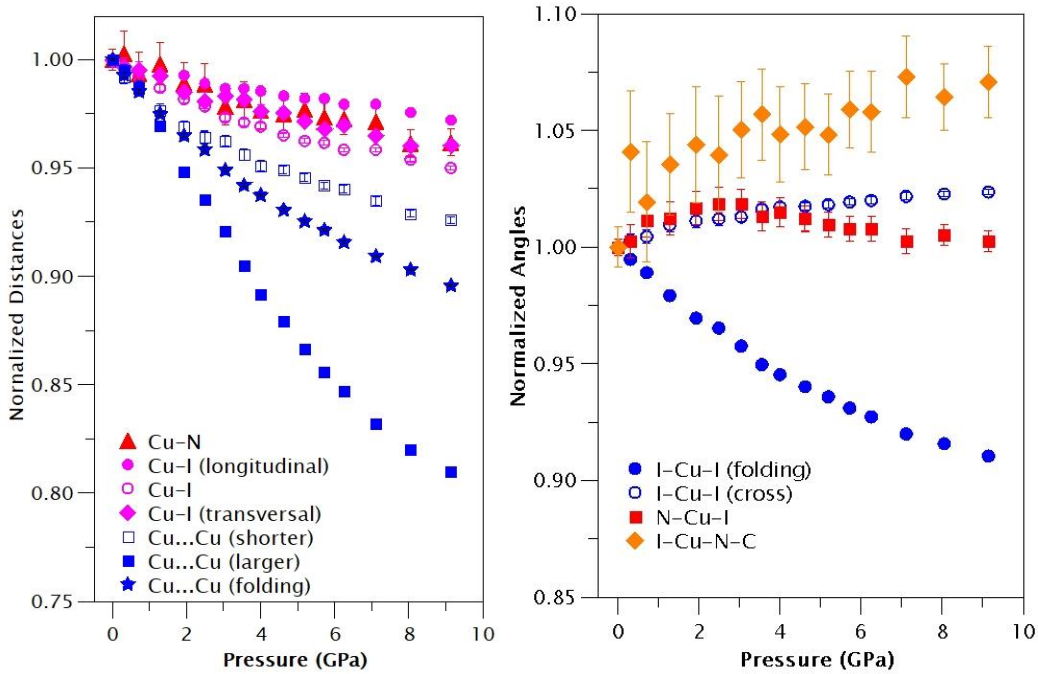

Figure S13. Behavior of the main bond distances and angles with pressure. Error bars represent the standard deviation for each value.

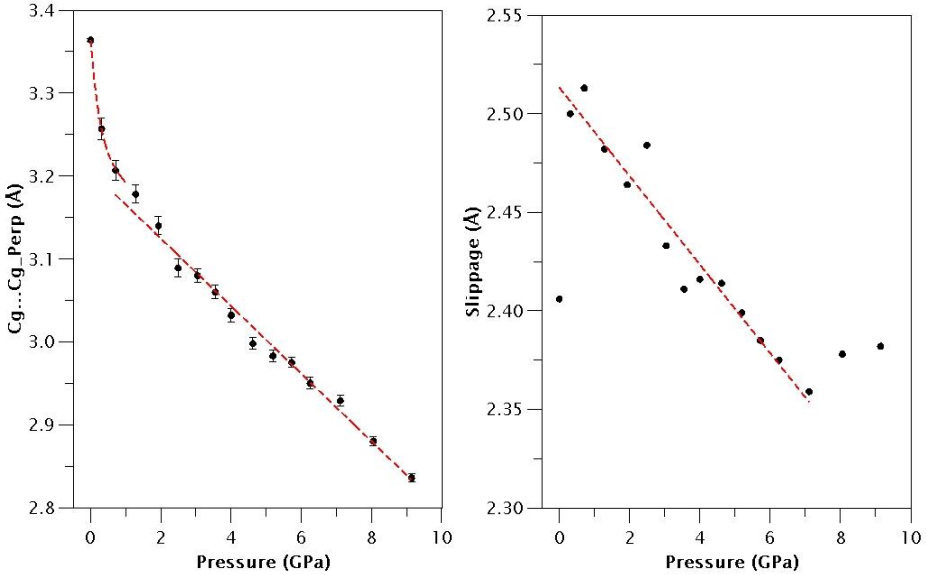

Figure S14. Perpendicular distances between pyrimidine ring and their respective mutual slippage (in-plane component of relative displacement) with pressure.

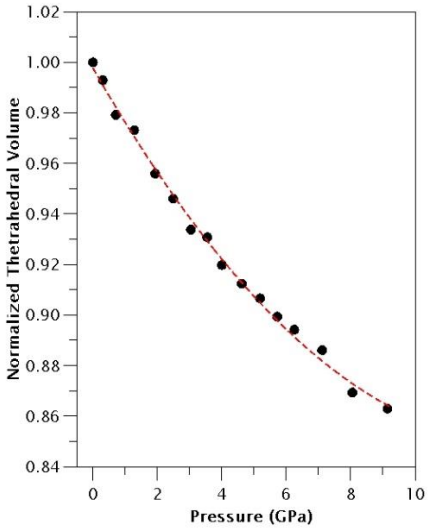

Figure S15. Tetrahedral volume as function of pressure.

EoS analysis for 1D-[Cu(aClpym)I]$_n$ (1).

In order to determine the order of the Birch-Murnaghan EoS model a *f-F* plot is shown (**Figure S16**). The positive linear slope indicates that the data have to be fitted using a 3rd-order.

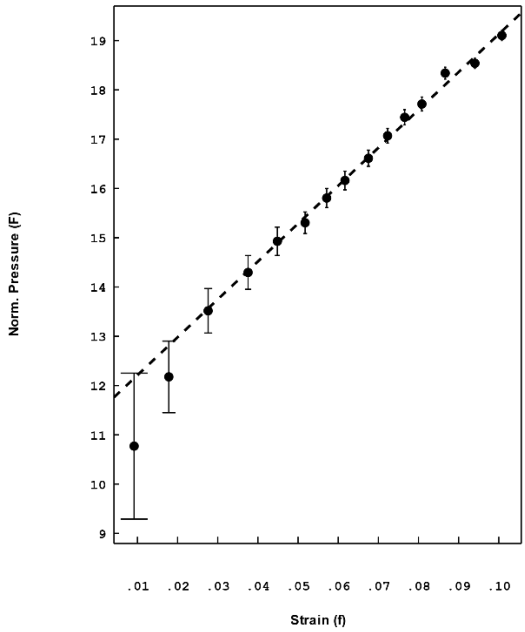

Figure S16. *f-F* plot for **1D-[Cu(aClpym)I]$_n$**. Dashed line represents the fitting EoS Model to BM3.

In **Figure S17** we can observe the behaviour of the volume with pressure. *f-F* plot confirms that we have to use a 3rd-order using the Birch-Murnaghan (BM) EoS.

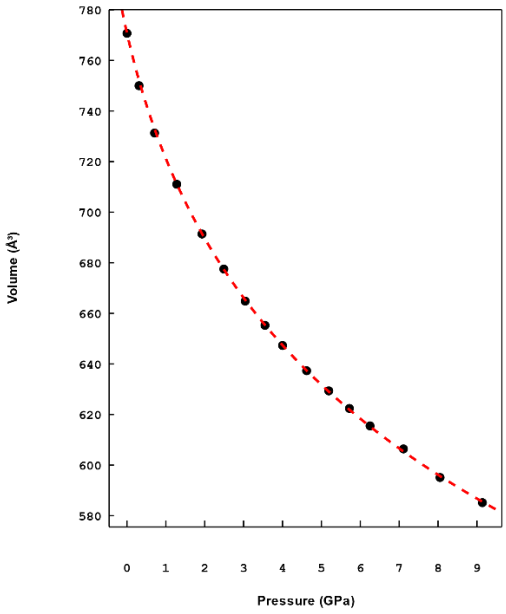

Figure S18. Volume behavior with pressure and their respective f-F plot. Dashed line represents the fitting EoS Model to BM3.

The volume *V*, and cell parameters (*a*, *b* and *c*) at equilibrium are displayed as V_0 and L_0, in **Table S7**, along with the linear moduli M_0 of each axis, the bulk modulus K_0 (both in GPa) and the bulk modules first derivative K'_0. The fitting procedure was done with the ***EosFit7-GUI*** program[1] using the BM EoS, with the linear modification of Angel *et al.* [2] used to fit individual cell parameters.

Table S7. EoS parameters for compound **1D-[Cu(aClpym)I]$_n$** (**CP1**)

	EoS Model	L_0	M_0	M'_0	M''_0
a	*BM3*	4.1357(4)	42.1(7)	12.2(3)	-0.843
b	*BM3*	16.817(2)	10.9(2)	53(1)	-165.022
c	*BM3*	11.1137(17)	91(4)	26(2)	-2.860
		V_0	K_0	K'_0	K''_0
V	*BM3*	770.71(6)	11.4(2)	8.5(2)	-2.464

The bulk modulus obtained for **1D-[Cu(aClpym)I]$_n$** falls into the range of 10-20 GPa typical for organometallic compounds [3,4] and similar values respect to the others Cu-I stair-case compounds. [5-6]

Optical changes under high pressure

The compound **1D-[Cu(Cldapym)I]$_n$** changed from colourless to brown (or dark yellow) with High Pressure as can be observed in **Figure S19**.

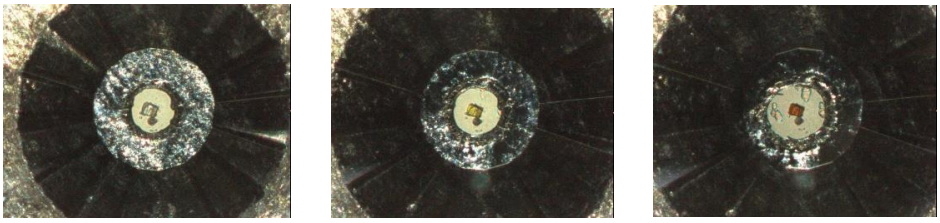

0.31GPa **4.63GPa** **9.14GPa**

Figure S19. Sample **1D-[Cu(aClpym)I]$_n$** inside of DAC at different pressures.

S6. Electrical behaviour study of 1D-[Cu(aClpym)I]$_n$.

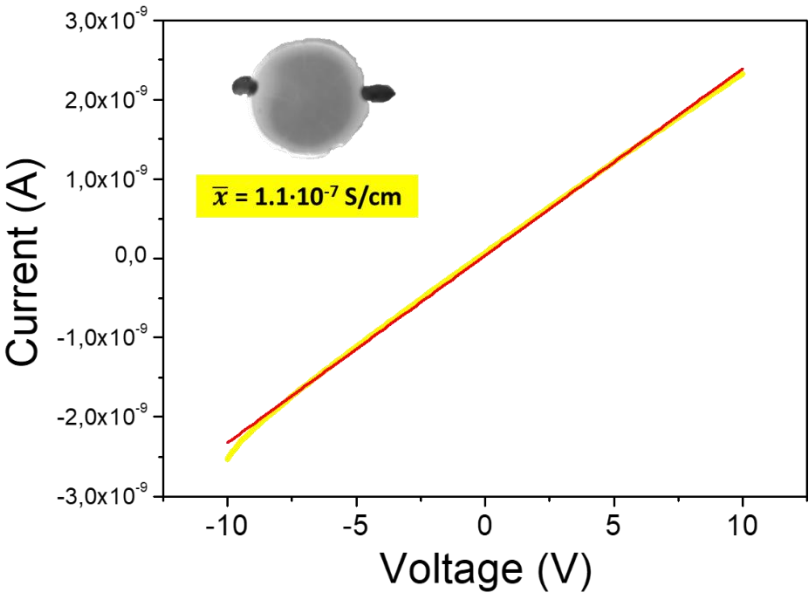

Figure S20. Graph of current intensity versus voltage of **1D-[Cu(aClpym)I]$_n$** in pressed pellet at 295 K.

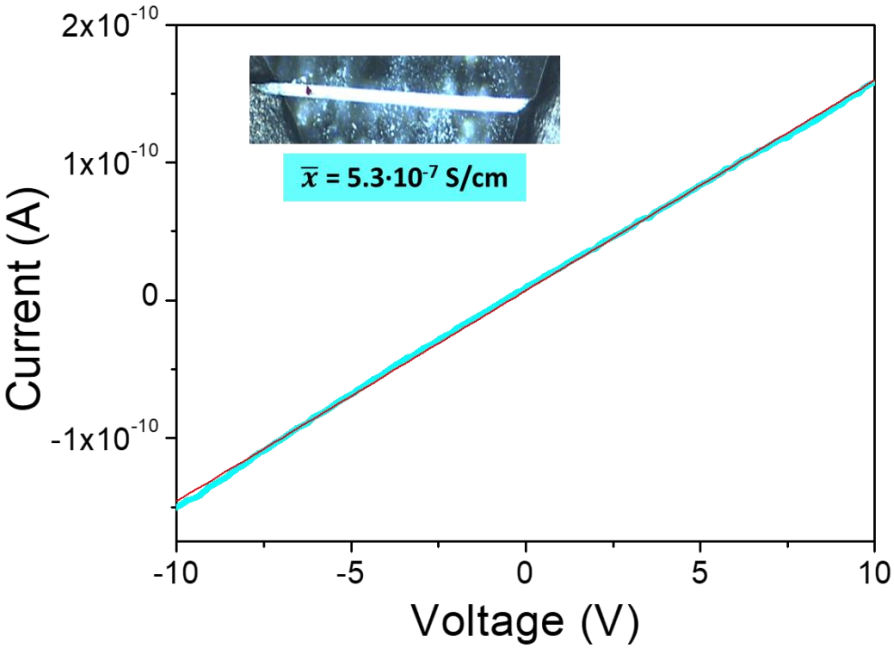

Figure S21. Graph of current intensity versus voltage of **1D-[Cu(aClpym)I]$_n$** in single crystal at 295 K.

S7. SEM Images

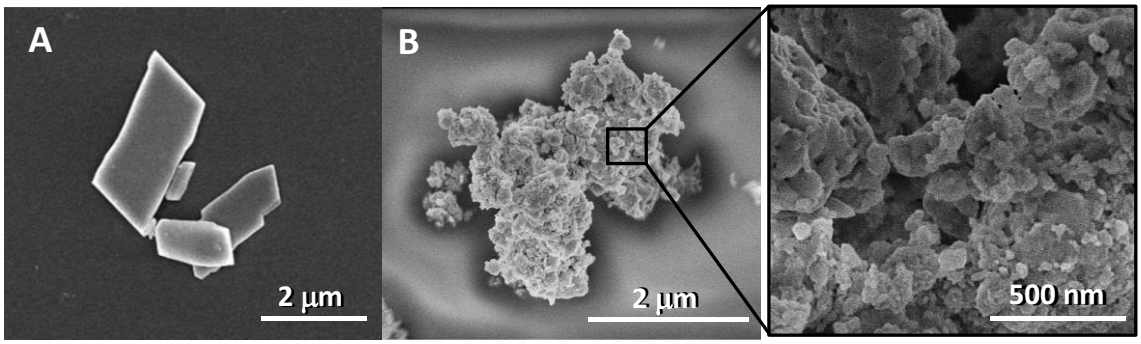

Figure S22. FESEM images of **1D-[Cu(aClpym)I]$_n$** polycrystalline without grinding (A) and grinded during 15 minutes (B).

S8. Diffuse reflectance UV-visible spectroscopy

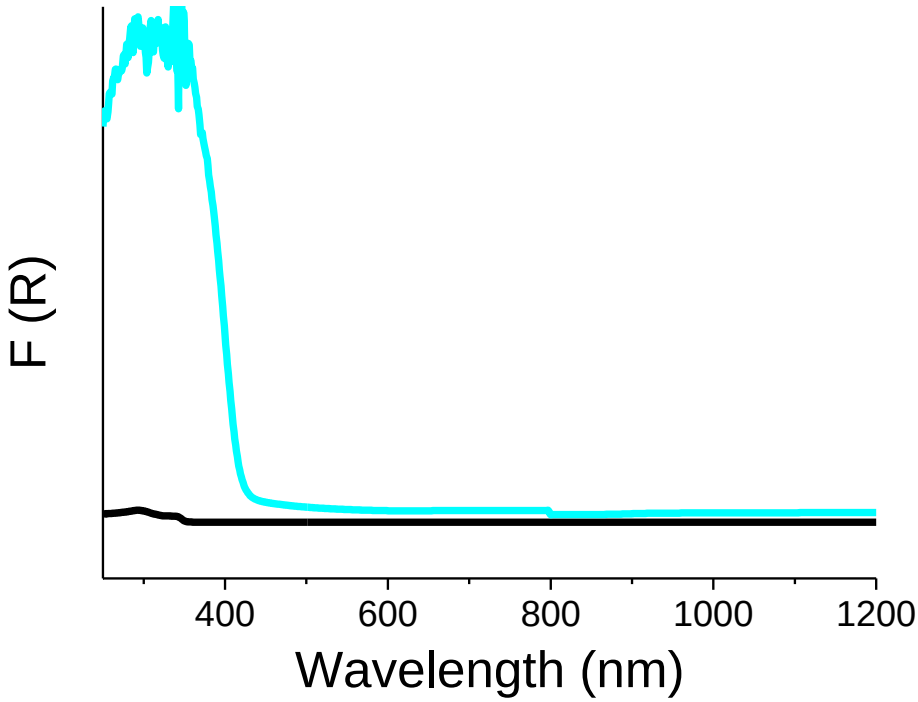

Figure S23. Diffuse reflectance UV-visible spectroscopy of aClpym (black line) and **1D-[Cu(aClpym)I]$_n$** (blue line).

1. Nestola, F.; Periotto, B.; Anzolini, C.; Andreozzi, G. B.; Woodland, A. B.; Lenaz, D.; Alvaro, M.; Princivalle, F., Equation of state of hercynite, FeAl2O4, and high-pressure systematics of Mg-Fe-Cr-Al spinels. *Mineralogical Magazine* **2015,** *79* (2), 285-294.
2. Angel, R. J.; Alvaro, M.; Gonzalez-Platas, J., EosFit7c and a Fortran module (library) for equation of state calculations. *Zeitschrift für Kristallographie - Crystalline Materials* **2014,** *229* (5), 405-419.
3. Spencer, E. C.; Ross, N. L.; Surbella, R. G.; Cahill, C. L., The influence of pressure on the structure of a 2D uranium(VI) carboxyphosphonoate compound. *Journal of Solid State Chemistry* **2014,** *218*, 1-5.
4. Funnell, N. P.; Dawson, A.; Francis, D.; Lennie, A. R.; Marshall, W. G.; Moggach, S. A.; Warren, J. E.; Parsons, S., The effect of pressure on the crystal structure of l-alanine. *Crystengcomm* **2010,** *12* (9), 2573-2583.
5. Conesa-Egea, J.; Nogal, N.; Martínez, J. I.; Fernández-Moreira, V.; Rodríguez-Mendoza, U. R.; González-Platas, J.; Gómez-García, C. J.; Delgado, S.; Zamora, F.; Amo-Ochoa, P., Smart composite films of nanometric thickness based on copper–iodine coordination polymers. Toward sensors. *Chemical Science* **2018,** *9* (41), 8000-8010.
6. Conesa-Egea, J.; González-Platas, J.; Rodríguez-Mendoza, U. R.; Martínez, J. I.; Pilar, O.; Fernández-Moreira, V.; Costa, R. D.; Fernández-Cestau, J.; Zamora, F.; Amo-Ochoa, P., Cunning defects: emission control by structural point defects on Cu(i)I double chain coordination polymers. *Journal of Materials Chemistry C* **2020,** *8* (4), 1448-1458.